Control and synchronization algorithms for a grid-connected photovoltaic system under harmonic distortions, frequency variations and unbalances

N. F. Guerrero-Rodríguez[a*], Alexis. B. Rey-Boué[b], Luis C. Herrero-de Lucas[c], Fernando Martinez-Rodrigo[d]

[a*] Department of Electronics, Computers Technology and Projects, Universidad Politécnica de Cartagena, c/Dr. Fleming, s/n 30202, Cartagena, Murcia, Spain. Tel.: +34 968 326514; fax: +34 968 326400, E-mail address: nestor.guerrero@upct.es

[b] Department of Electronics, Computers Technology and Projects, Universidad Politécnica de Cartagena, c/Dr. Fleming, s/n 30202, Cartagena, Murcia, Spain. Tel.: +34 968 325928; fax: +34 968 326400, E-mail address: alexis.rey@upct.es

[c] Department of Electronics Technology, Universidad de Valladolid, c/Fco. Mendizabal 1, 47014, Valladolid, Spain. Tel.: +34 983 423521; fax: +34 983 423490, E-mail address: lcherrer@tele.uva.es

[d] Department of Electronics Technology, Universidad de Valladolid, c/Fco. Mendizabal 1, 47014, Valladolid, Spain. Tel.: +34 983 423921; fax: +34 983 423490, E-mail address: fer_mart@tele.uva.es

*Corresponding autor: N. F. Guerrero-Rodríguez

ABSTRACT

In this paper, an implementation of the control and the synchronization algorithms for a Voltage Source Inverter used as the power conditioner for Photovoltaic renewable energy in a grid-connected structure is carried out. Its main purpose is to show, in a simple manner, the design and **combined operation** of the control and synchronization algorithms for attaining the proper behaviour of the Grid Inverter when the 3-phase utility grid is disturbed by voltage unbalances, frequency variations and harmonic distortions, according to **power quality standards**.

In order to obtain a high efficiency of the system during perturbations, a **Proportional Resonant** controller with a **Harmonic Compensator** structure is designed for the control algorithm, whereas a Dual Second Order Generalized Integrator Frequency-Locked Loop (**DSOGI-FLL**) is used as the synchronization algorithm.

In order to validate both the control and the synchronization algorithms, some simulations using MATLAB/SIMULINK from The MathWorks, Inc. are shown firstly, and secondly, some real-time digital simulations are carried out.

Keywords: Photovoltaic Agent, DSOGI-FLL, Real-Time Digital Simulation, Proportional Resonant, Harmonic Compensator.

1. INTRODUCTION

In the framework of a Distributed Generation (DG) system, the connection of new, clean and infinite renewable agents to the utility grid, as an alternative to traditional ones [1] for the collaborative effort towards the mitigation of the greenhouse effect [2], must be properly controlled according to the expected operating conditions of the primary energy as well as the utility grid normative. For example, different values of irradiance, temperature variation, and islanding protections are taken into account when dealing with grid-connected Photovoltaic (PV) agents, as well as the control of the power factor (PF) of the inverter-grid connection [3]. In addition, the good power quality [4] according to international standards [3,5-7] must always be observed.

Regarding the harmonic regulations, a limit of 5% for the Total Harmonic Distortion (THD_I) is established for the grid currents [7-9] and a current regulator for the 3-phase inverter currents is mandatory, meanwhile the PF control is achieved with a synchronization algorithm which detects the phase angle of the 3-phase utility grid voltages with optimal dynamic response.

Previously, grid codes have allowed PV generators disconnection in the case of grid faults, but the PV power installed in Europe has been growing continuously because the cells prices are dropping, and nowadays the PV generators can destabilize the grid if they are disconnected under grid faults. So, the European countries are changing their grid codes, Germany and Italy already did it, to increase the capability of PV generators in helping to stabilize the grid. The new codes for medium and low voltage connection of PV power include fault-ride-through capability, voltage support by means of reactive current injection and frequency dependence [10].

PV modules produce dc electric quantities and a power conditioning system is needed to convert these dc quantities into ac ones [11-13], as well as to balance the power flow between the renewable agent and the utility grid. For 3-phase systems, it is mandatory to exert a decoupled control of the instantaneous active and reactive powers of the inverter-grid connection [14]. Voltage Source Inverters (VSI) are commonly used as the power conditioner units to interface renewable resources to the utility grid in a Distributed Generation (DG) framework [11,15], and are built with semiconductor devices operating in switch-mode.

Several publications have studied and analyzed the control and synchronization algorithms separately [13,16-18], and in this paper a **combined operation** of both algorithms is studied so as to validate its performance and to ensure the higher efficiency of the PV grid-connected system when the 3-phase utility grid is affected by voltage unbalances, variations of its nominal frequency and low order harmonics. For this, the Dual Second Order Generalized Integrator Frequency Locked Loop **(DSOGI-FLL)** proposed in [13,18] is used as the synchronization algorithm together with the **Proportional Resonant (PR)** controller and a **Harmonic Compensator (HC)** structure proposed in [19].

Section 2 of this paper is focused on the study of grid-connected PV systems: the main parts of the control and power subsystems will be described with more emphasis on the DSOGI-FLL and the PR controller. **Section 3** describes the case of study of a 10kW grid-connected PV renewable agent system that will be used to validate the control and the synchronization algorithms under several disturbance conditions. In **Section 4**, the global performance of the PV renewable agent will be studied with several simulations using MATLAB/SIMULINK tool [20]. In **Section 5**, real-time digital experiments will be performed using a DS1006 DSPACE platform with several I/O, ADC and DAC blocks in order to reinforce the validity of the previous study. Finally, some conclusions are shown in **Section 6**.

Nomenclature

v_p	output voltage of the PV Generator	v_r, v_s, v_t	3-phase utility grid voltages
i_p	output current of the PV Generator	S_u, S_v, S_w	state of the power-poles
P_{PV}	power in the PV generator	$\mathbf{u}$	inverter voltage space vector
v_{CC}	dc bus voltage	$\mathbf{i}$	inverter line current space vector
v^{*}_{CC}	dc bus voltage reference	$\mathbf{u}_{AC}$	utility grid voltage space vector
i_{CC}	current that will be injected into the inverter	L	line inductance
C_{link}	dc-link capacitor	R	resistance of the line inductance
i_{clink}	current through the dc-link capacitor	v_{α}, v_{β}	$\alpha\beta$ components of space vector **u**
θ	phase of the 3-phase utility grid voltages	i_{α}, i_{β}	$\alpha\beta$ components of space vector **i**
ω	fundamental angular frequency	$u_{ac\alpha}, u_{ac\beta}$	$\alpha\beta$ components of space vector $\mathbf{u}_{AC}$
i_u, i_v, i_w	3-phase inverter line currents	p	instantaneous active power
i_r, i_s, i_t	3-phase utility grid currents	q	instantaneous reactive power
DQ	in-quadrature signals	i^{*}_{d}, i^{*}_{q}	*d-q* reference components of vector $\mathbf{i}^{*}$
ω'	estimated angular frequency	q^{*}	instantaneous reactive power reference
ω	angular frequency	PI_{VCC}	voltage PI regulator
k	gain of the SOGI block	F_{sw}	switching frequency
K_I and K_P	constants of the voltage PI regulator	t_S	settling time
		τ	time constant of the first order system
		$t_{S(FLL)}$	settling time of the FLL
		Γ	gain to set $t_{S(FLL)}$

2. GRID-CONNECTED PV SYSTEM

For PV grid-connected systems, it is necessary to control the power flow between the primary renewable energy source and the utility grid [19], as well as the power factor of the inverter-grid connection with high power quality [21]. The power conditioner, working in inverter-mode (3-phase Voltage Source Inverter (VSI)), must guarantee the maximum efficiency by injecting the maximum available power at the PV module into the utility grid, as well as by controlling the power factor of the inverter-grid connection; the latter makes use of the instantaneous reactive power theory [22] for 3-phase systems which allows the control of the instantaneous active and reactive powers in decoupled axes [14]. The global 3-phase PV grid-connected system can be divided into two subsystems [21], the power and the control subsystems, whose block diagram is depicted in Fig. 1.

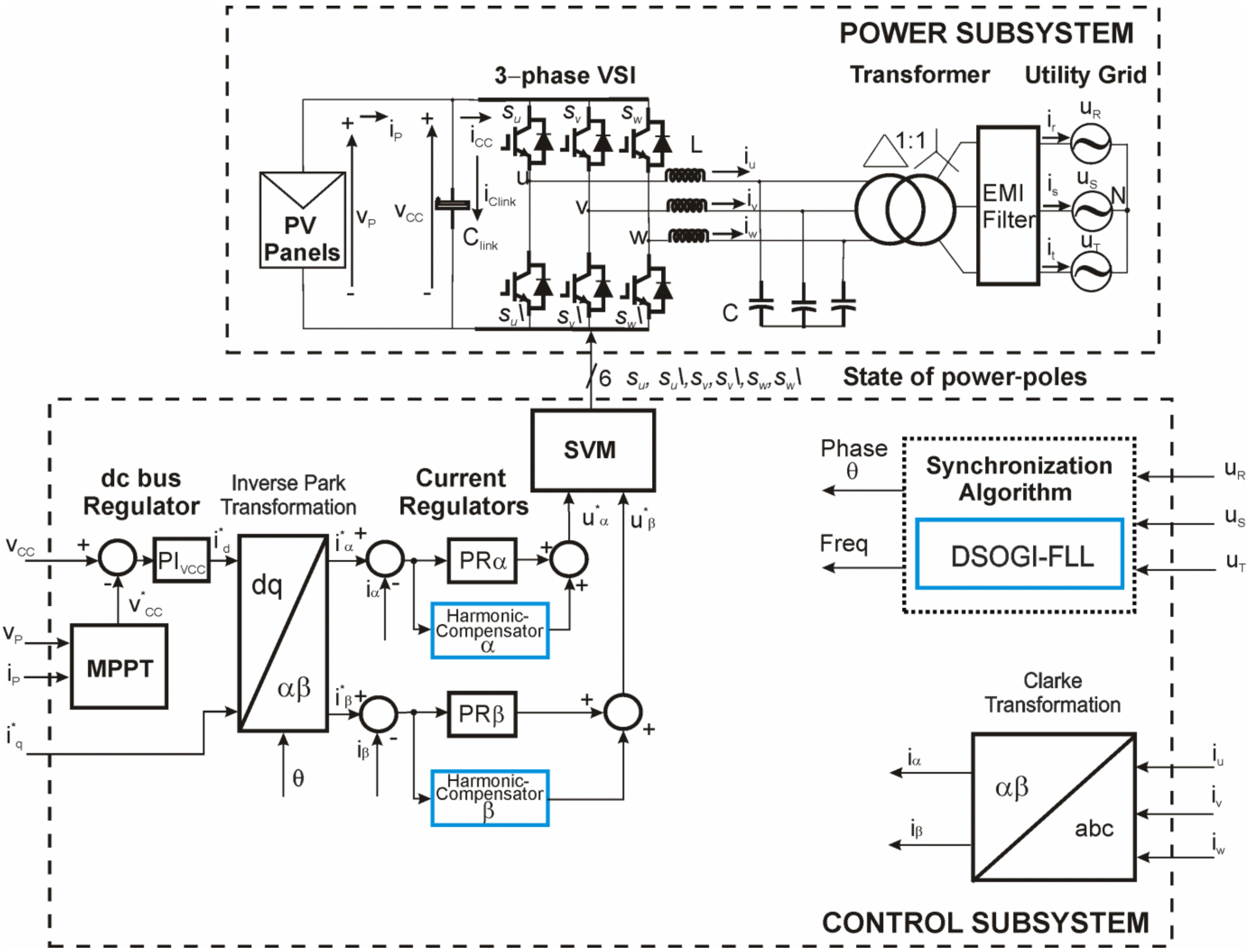

Fig. 1. Block diagram of the Power and Control Subsystems for a 3-phase grid-connected system.

2.1 Power Subsystem

The power subsystem is formed by the PV modules, the inverter, the LCL and the EMI filters. The LCL filter and the 3-phase utility grid are configured as a three wire system with two degrees of freedom.

The PV modules supply the incoming power, according the available solar irradiance [23] and the cell temperature, into the utility grid, and its size (arrange of parallel-series PV cells) will depend of the required power of the PV system [24].

The mission of the inverter, mainly built with semi-conductor electronic devices [12] (IGBTs and diodes), is to convert the generated dc voltage into suitable ac currents to be fed into the 3-phase low-voltage utility grid [11]. Pulse-width modulation (PMW) and space vector modulation (SVM) techniques are used to control the gate signals of power switches according to the averaged voltage and current references.

According to Fig. 1, the dc side of the inverter can be described as follows:

$$
\begin{aligned}
i_p &= i_{clink} + i_{CC} \\
i_{CC} &= s_u \cdot i_u + s_v \cdot i_v + s_w \cdot i_w \\
i_{clink} &= C_{link} \frac{dv_{CC}}{dt} \\
P_{PV} &= i_p v_p
\end{aligned} \tag{1}
$$

where v_p, i_p are the voltage and the output current of the PV generator, respectively, P_{PV} is the available power for a specific irradiance and cell temperature, v_{CC} is the dc bus voltage, i_{clink} is the current through the link capacitor C_{link}, and i_{CC} is the current delivered to the 3-phase VSI (which is a function of the line currents i_u, i_v, i_w and the states of the power-poles s_u, s_v, s_w (1:'on', 0:'off', s_i-upper pole, $s_i\backslash$-lower pole in the 3-phase VSI).

Neglecting the effect of the inductance of the isolation transformer and the EMI filter at the fundamental and low frequencies, the voltages at the filter capacitors are approximately the same as in the three phase utility grid voltages. Defining a generic 3-phase system [x_1 x_2 x_3], where x_1 x_2 x_3 are the instantaneous 3-phase variables, its corresponding generic space vector **x** can be stated as **x**= [x_1 x_2 x_3]^t, and the dynamic in the ac side of the inverter can be expressed in a vector way as follows:

$$
\mathbf{u} - \mathbf{u_{AC}} = R\mathbf{i} + L\frac{\mathbf{di}}{\mathbf{dt}} = \mathbf{u_R} + \mathbf{u_L} \tag{2}
$$

where **u**, **i**, $\mathbf{u_{AC}}$ are the inverter voltage, the inverter line current and the utility grid voltage space vectors of its corresponding instantaneous 3-phase variables, respectively; *L* is the line inductance and its cupper resistance *R*.

Neglecting the losses of the distribution transformer and the EMI filter and expressing the last vector equation with its $\alpha\beta$ components using the Clarke Transformation [25] (see Appendix A for the transformation matrices), the power flow between the 3-phase VSI and the utility grid can be deduced by using the instantaneous reactive power theory [26]. So, the instantaneous active power (p) and the instantaneous reactive power (q) can be expressed as follows [22,27]:

$$
p = v_{ac_\alpha} i_\alpha + v_{ac_\beta} i_\beta \tag{3}
$$

$$
q = v_{ac_\beta} i_\alpha - v_{ac_\alpha} i_\beta \tag{4}
$$

where v_{ac_α}, v_{ac_β}, i_α and i_β are the $\alpha\beta$ components of 3-phase voltages and currents, respectively.

In addition of guaranteeing a constant power delivery to the 3-phase utility grid, PV renewable agents must fulfill the power quality regulations. The maximum total harmonic distortion (THD) for the 3-phase currents must be around 5% [9] according to several normative [7,8], whereas the normative for the low order harmonic distortions is indeed more restrictive. A resume of different standards about power quality for photovoltaic systems can be found in [28]. Ripples are created in the output currents of the inverter due to the high frequency commutation of the IGBTs, meanwhile the low order harmonics are produced by non-linear loads. The best solution for correcting the high frequency ripples is by using an LC or an LCL filter [29] in the ac side of the inverter, meanwhile the amplitude of the low order harmonic must also be attenuated to guarantee a good power quality injection to the utility grid, although this a difficult task except if a harmonic-compensator (HC) algorithm is used.

In a grid-connected PV renewable agent, it is necessary to take into account the harmonic pollution due to the Electromagnetic Interference (EMI). These EMIs are caused by the semiconductor electronic devices (IGBTs and diodes) [30] and an EMI filter is needed to reduce it. There are too many methodologies to design the appropriate EMI filter, some of them are based on trial and error [30,31], and some novel methodologies are cited in several publications, including [31,32].

2.2 Control Subsystem

The control subsystem is formed by the Maximum Power Point Tracking (MPPT) algorithm, the synchronization algorithm, and the outer voltage PI and the inner current PR regulators.

The MPPT [33] is an essential algorithm-module of a PV system for extracting the maximum available power of the PV modules [34] in order to increase the efficiency of the system [14]. The study of the MPPT algorithm is out of the scope of this paper, but interested readers may find some additional information in the scientific literature, such as [34-39].

2.2.1 Synchronization algorithm

The synchronization algorithm for attaining a controllable power factor in the connection must detect the phase of the 3-phase utility grid voltages with optimal dynamic response. However, the measured signals can be contaminated with harmonics, voltage unbalances, and frequency variations [40]; also, the used sensors can introduce second order harmonics due to accuracy errors.

Classical dqPLL method (in the synchronous reference frame) for synchronization is very sensible to grid voltage unbalances, which also produce second order harmonics in the dc bus voltage [41]. To overcome this fact, a Positive Sequence Detector (PSD) block, based on the symmetrical component method or Fortescue theorem [42], is added to extract the positive sequence of the 3-phase utility grid voltages, yielding the PSD+dqPLL synchronization algorithm [43]. However, due to the discrete filter named S90 [43] used in the PSD block this algorithm could be sensitive to the variation of the nominal frequency of the utility grid [44] and may lead to the power factor degradation of the inverter-grid connection.

A solution for the frequency and phase detections when voltage unbalances and frequency variations occur in the 3-phase utility grid voltages is described in [13], where a Dual Second Order Generalized Integrator FLL (DSOGI-FLL) is proposed for the $\alpha\beta$ voltage components ($v_{\alpha\beta}$) in the stationary reference frame. In this, the in-quadrature signals (90^{o} shifted) for $v_{\alpha\beta}$ are computed by two Second Order Generalized Integrator [45] with a Quadrature Signal Generation (SOGI-QSG) [18], one of them shown in Fig. 2.

The block diagram of the SOGI, which behaves as an integrator with infinite gain, is depicted in **blue** and its transfer functions is described by Eq. (5).

$$SOGI(s) = \frac{v'}{k\varepsilon_v}(s) = \frac{\omega' s}{s^2 + \omega'^2} \quad (5)$$

whereas the transfer functions of the in-quadrature signals DQ are described by Eq. (6) and (7).

$$D(s)=\frac{v'}{v}(s)=\frac{k\omega' s}{s^2+k\omega' s+\omega'^2} \tag{6}$$

$$Q(s)=\frac{qv'}{v}(s)=\frac{k\omega'^2}{s^2+k\omega' s+\omega'^2} \tag{7}$$

ω' is the centre angular frequency of the adaptive filter, and k is the gain of the SOGI block. The transfer functions described by Eq. (6) and (7) suggest a band-pass and a low-pass filter behaviour, respectively, and Eq. (7) implies a constant lag of 90º between the qv' and v which will not be a function of the variation of ω' and k [18], yielding also to an insensitive system for frequency variations at the input signal v when $\omega=\omega'$ (ω is the angular frequency of v).

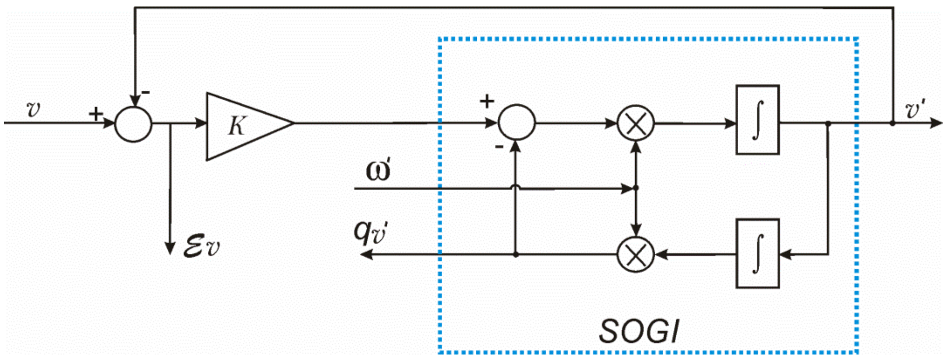

Fig. 2. Block diagram of a SOGI-QSG.

Equations (6) and (7) are second order transfer functions, and its dynamic response will depend on the localization of the poles in the complex plane. In addition, the band-pass and low-pass filter behaviour described above suggest the harmonic rejection capability of these filters. So, a trade-off between the proper bandwidth for harmonic rejection, and the proper settling time with the corresponding overshoot for the dynamic response, must be imposed for the calculation of k for a specific ω'.

Figure 3a shows the Bode plot of the transfer functions of the SOGI-QSG described by Eq. (6) and (7): the upper zone of Fig. 3a shows the magnitude of the Bode plot, meanwhile the bottom zone shows the phase angle, both for several values of k. The trace of the phase depicts a perfect 90º shifting between the in-quadrature signals for all k. In addition, Fig. 3b depicts the time evolution of the in-quadrature signals and the corresponding settling times for all k.

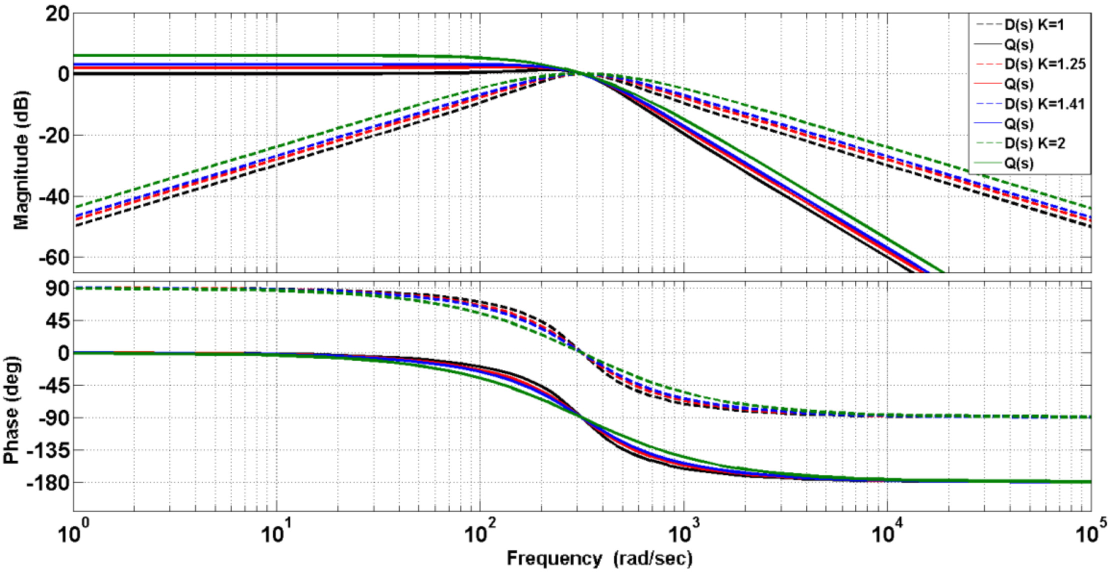

(a)

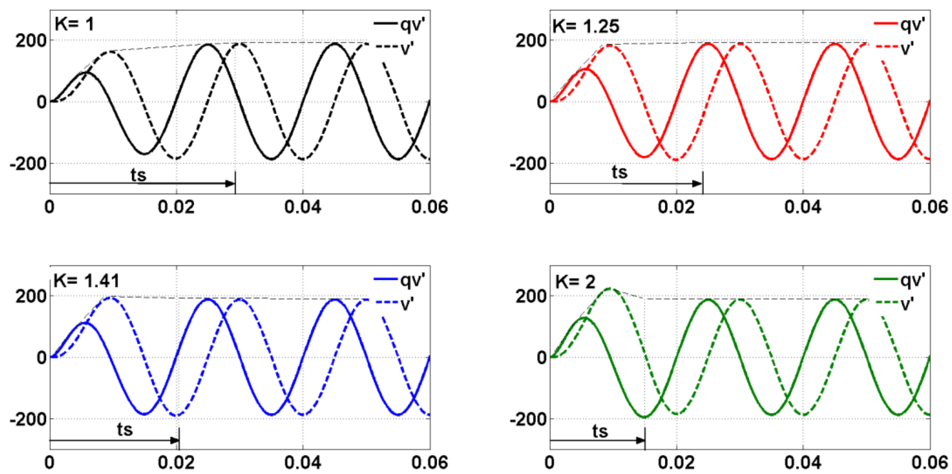

(b)

Fig. 3. a) Bode plot of a SOGI-QSG using the transfer functions of Equations (6) and (7) for several values of k.
b) Time evolution of the in-quadrature signals of the SOGI-QSG for several values of k.

Table 1 resumes the influence of gain k in the SOGI-QSG behavior according to the settling time, overshoot, damping factor, and harmonic rejection of Q(s): when k increases, the settling time and the harmonic rejection decreases, but the overshoot increases instead. It must be observed that when k =1.414, a good trade-off between the harmonic rejection (for the 5th and 7th harmonics) and the dynamic response is achieved, corresponding to a damping factor $\zeta_{SOGI-QSG}$ =0.707 for second order systems [46].

Table 1. SOGI-QSG behavior according gain k.

k	$\zeta_{SOGI-QSG}$	Overshoot (%)	Settling time (ms)	Harmonic Rejection of Q(s) (dB)	
				5th	7th
1	1	0	29.3	-27.72	-33.7
1.25	0.8	1.5	23.4	-25.89	-31.81
1.414	**0.707**	**4.3**	**20.7**	**-24.9**	**-30.78**
2	0.5	16.3	14.6	-22.23	-27.94

It must be pointed out that the SOGI-QSG synchronization algorithm is tuned to the centre angular frequency ω', which is an input signal to this block (see Fig. 2), and can behave as an adaptive filter scheme if an external circuit or algorithm is able to measure or detect this frequency. The Frequency Locked Loop (FLL) structure, shown in Fig. 4 [18], can be used to measure the angular frequency ω of the input signal v (in this case, ω' is the output or estimated angular frequency of the input signal v) without using trigonometric functions [18], and making easier its implementation in conventional microcontrollers. The nominal angular frequency ω_c is feed-forward to this block in order to improve the dynamic response of the algorithm.

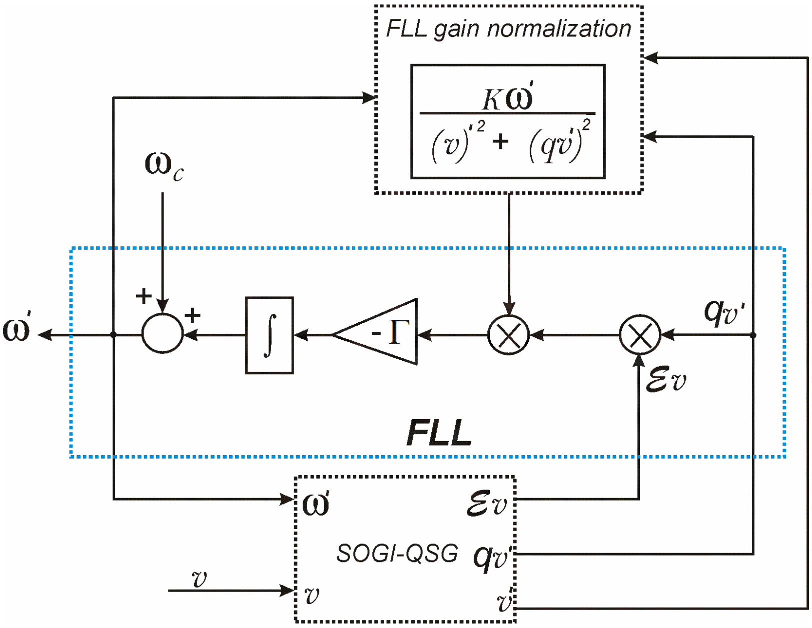

Fig. 4. Block diagram of a Frequency-Locked Loop (FLL) with gain normalization.

A FLL gain normalization is exerted so as to make this independent of the gain k of the SOGI-QSG block and of the amplitude of the utility grid voltage. In this case, the FLL algorithm can be approximated by a first order system with one integrator for steady state operation and linearized around the nominal output variables of the SOGI-QSG block. So, the settling time t_s can be set approximately by 5τ ($\tau = \frac{1}{\Gamma}$ is the time constant of the first order system):

$$t_{s(FLL)} \approx \frac{5}{\Gamma} \quad (8)$$

Finally, the measurement of ω' implies the feedback of the qv' signal from the SOGI-QSG block. This signal will have a small amount of harmonic contamination due to the attenuation imposed by the low-pass filter nature of the transfer function Q(s) described by Eq. (7).

The preliminary analysis can be extended to 3-phase systems, and Fig. 5 shows the DSOGI-FLL structure proposed in [18]. Clarke transformation [25] is applied to the input 3-phase voltages in order to obtain its $\alpha\beta$ voltage components ($v_{\alpha\beta}$), and two SOGI-QSG blocks are used to obtain its in-quadrature signals. Knowing that the instantaneous positive sequence component ($v_{\alpha\beta}^{+}$) of a voltage vector described by $v_{\alpha\beta}$ is given by [47]:

$$v^{+}_{\alpha\beta} = \frac{1}{2}\begin{pmatrix} 1 & -q \\ q & 1 \end{pmatrix} v_{\alpha\beta} \qquad (9)$$

where $q = e^{-j\frac{\pi}{2}}$ is a phase-shift operator to obtain the in-quadrature version of an original wave form, a Positive Sequence Calculator (PSC) must be designed and applied to the in-quadrature output signals so as to compute the positive sequence of the input 3-phase unbalanced voltages $v_{\alpha\beta}^{+'}$.

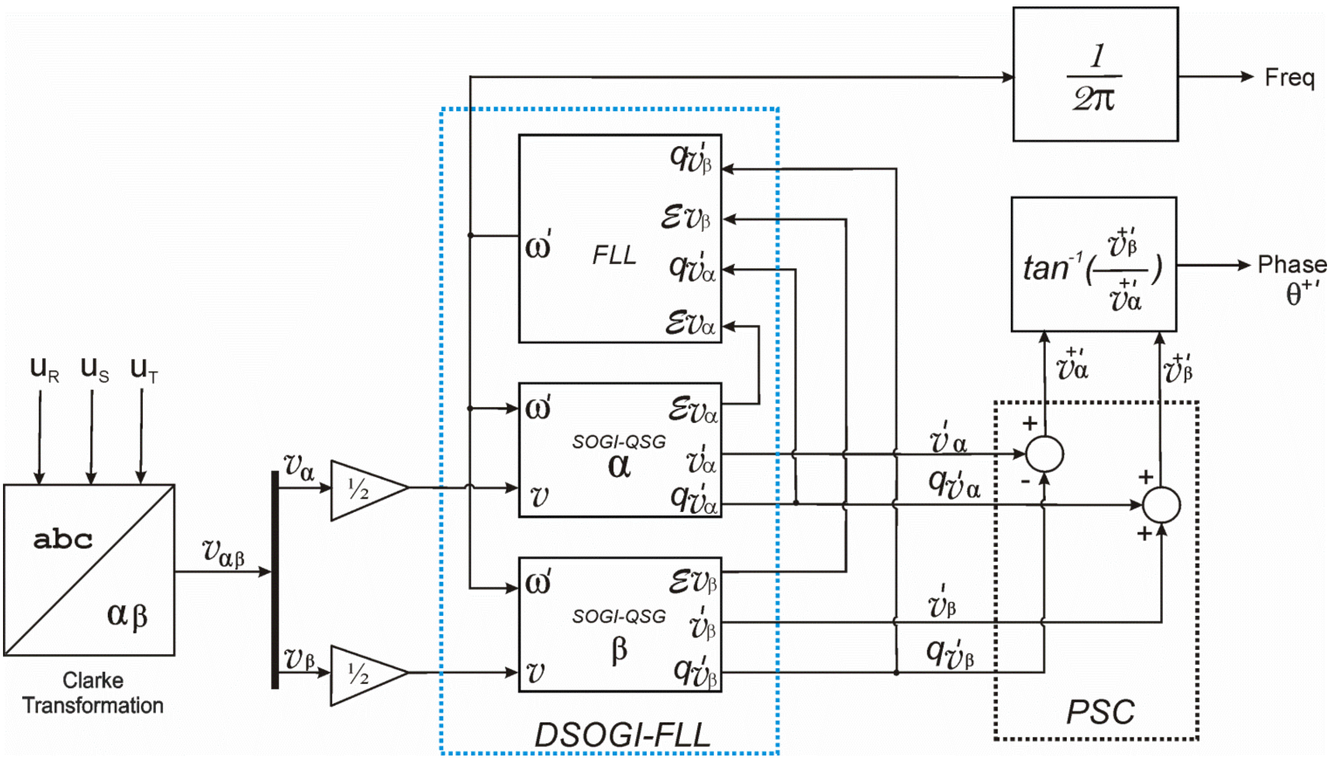

Fig. 5. Block diagram of a DSOGI-FLL synchronization algorithm.

Finally, the phase angle for the positive sequence of the 3-phase utility grid voltages can be computed as follows:

$$\theta^{+'} = \tan^{-1}\left(\frac{v_{\beta}^{+'}}{v_{\alpha}^{+'}}\right) \qquad (10)$$

In order to evaluate the performance of the DSOGI-FLL structure, some simulations depict the time evolution of the detected frequency in Fig. 6. A step of 50-60Hz is exerted in the nominal frequency of the 3-phase utility grid voltages and several gains (Γ) are imposed to study the dynamic response. Using a relatively low Γ (50 and 70) a slow settling time of the FLL is attained (trace in **red** and **blue**). On the contrary, for Γ = 100 (trace in **black**), a suitable settling time around two cycles and a half is achieved.

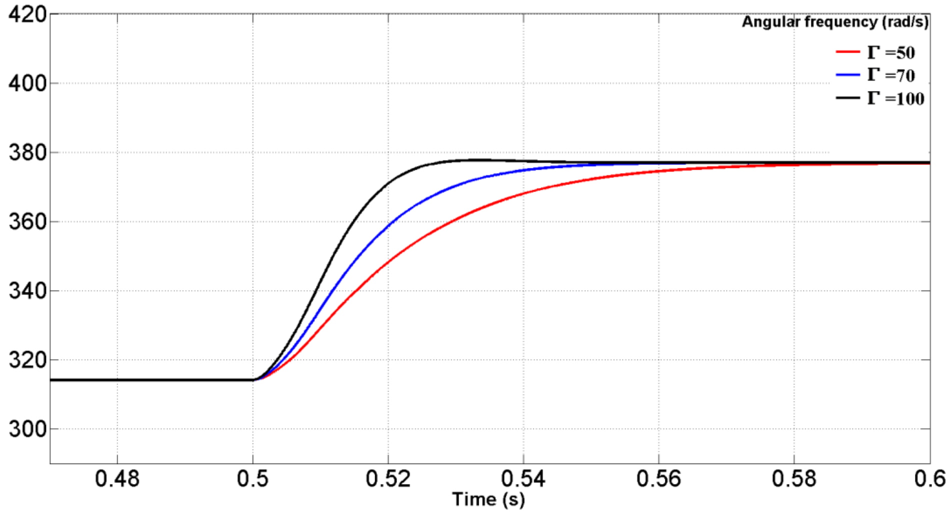

Fig. 6. Time response of the DSOGI-FLL for several Γ.

Table 2 show the relation between the gain Γ and the corresponding settling time $t_{s(FLL)}$ when a step of frequency of 50Hz to 60Hz is exerted on the utility grid frequency.

Table 2. Relation between the gain Γ and $t_{s(FLL)}$ in the FLL block.

Γ	$t_{s(FLL)}$ (ms)
50	100
70	70
100	**50**

2.2.2 *Cascade control*

The control strategy uses a cascade control: the outer voltage and the inner current regulators.

The outer loop regulator compares the dc bus voltage in the link capacitor with the reference which comes from the MPPT algorithm block, keeping a constant dc voltage and assuring the power flow balance between the PV system and the utility grid. This control loop has been performed using a PI regulator whose output is the reference *d* component of the inverter 3-phase currents (i^*_d) in the synchronous reference frame (dq) (see Appendix A), meanwhile the reference *q* component (i^*_q) is set in an open loop scheme for the power factor control of the inverter-grid connection. The PI regulator constants, K_I and K_P, are calculated under the recommendations described in [21,48] which suggests a phase margin PM_V=63.5° for assuring the best trade-off between the relative stability, the overshoot and the settling time of the system.

Classical PI regulators produce zero steady-state error for dc signals due to its integral part. In a similar way, when sinusoidal signals are to be regulated, Proportional Resonant (PR) regulators must be used instead for zero steady-state error behaviour, and the resonant part can be viewed as a generalized integrator (GI) [45]. In addition, for 3-phase unbalanced systems (three wire configuration), two PR controllers can perfectly track both the positive- and the negative- sequence of the 3-phase sinusoidal references, and reject the 3-phase sinusoidal disturbances according to the internal model principle (see appendix C of [13] for a detailed explanation of this principle) because its transfer functions have a pair of conjugate poles in the complex plane at the fundamental resonance angular frequency (ω_0 and $-\omega_0$).

Applying the inverse Park Transformation (see Appendix A) to i^*_d and i^*_q computes the sinusoidal reference currents i^*_α, i^*_β. Clarke transformation (abc->$\alpha\beta$) are applied to the 3-phase line currents, computing its sinusoidal $\alpha\beta$ components which are compared with i^*_α, i^*_β, and the errors are fed to the two PR controllers in the Stationary Refrence Frame (αβ), whose outputs are the average reference sinusoidal inverter voltage ($u^*_{\alpha\beta}$). This inner current loop is closed with the SVM block which decides the state of the power-poles of the 3-phase inverter, allowing the synchronization of the inverter line currents with the utility grid voltages with zero error at steady-state, and also rejecting the disturbance produced by the 3-phase utility grid voltages which avoids the necessity of applying a feedforward open-loop control scheme.

The ideal and the non-ideal PR controllers are described in [16], in which the former has an infinite gain within a narrow bandwidth around the fundamental resonance angular frequency ω_0, which may lead to stability and digital implementation problems, meanwhile the latter adds the cut-off frequency ω_c, which leads to a high but finite gain, solving the stability problems and allowing an easier digital implementation.

The non-ideal PR controller will be used in this paper, whose transfer function is described by Eq. (11). The dynamic of the system in terms of bandwidth, phase and gains margin will depend of the proportional gain K_P which is adjusted in a similar way as it is tuned in a PI controller; the steady-state error will depend of the integral gain K_I whose value will be selected comparatively high, but holding the limits for stability, and ω_c must be set empirically to 5-15 rad/s with good results [16].

$$G_{PR}(s) = K_P + \frac{2K_I\omega_c s}{s^2 + 2\omega_c s + \omega_0^2} \qquad (11)$$

Cascading multiple genaralized integrators (GI) tunned to resonate at specific low order harmonic angular frequencies $h\omega_0$ with the PR controller described above [41], enables the Harmonic Compensator (HC) structure for the rejection of the low-frequency harmonic perturbances of the 3-phase utility grid voltages according to the internal model principle mentioned above. Then, a good power quality can be delivered into the utility grid with minimal computational burden.

The transfer function of the HC is described by Eq. (12), where h is the harmonic to be compensated, and K_{Ih} , ω_{ch} can be adjusted in a similar manner as in the non-ideal PR controller.

$$G_h(s) = \sum_{h=5,7} \frac{2K_{Ih}\omega_{ch} s}{s^2 + 2\omega_{ch} s + (h\omega_0)^2} \qquad (12)$$

Finally, the generic PR controller and the HC structure are described in Fig. 7 for the 5th and 7th harmonics, but it can be easily extended to any other low-frequency harmonic perturbation.

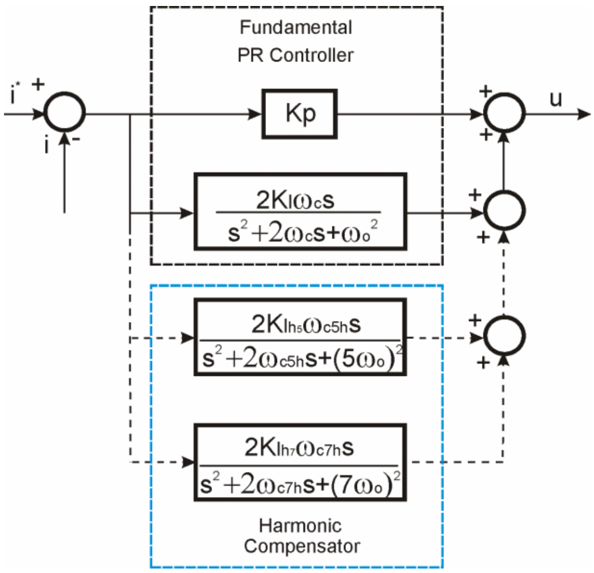

Fig. 7. PR + Harmonic Compensator structure.

3. CASE OF STUDY

A PV grid-connected system of 10kW of nominal power at standard conditions (1000 W/m^2 and 25 °C) [49] will be studied. The chosen parameters are based on a 3-phase inverter built with the 6-pack-integrated intelligent Power System SKIIP 513GD172-3DUL from SEMIKRON, which includes the IGBTs semiconductors for the 3-phase power-poles, and configured to work at 12.208KHz of PWM switching frequency (F_{PWM}=12.208kHz (244th harmonic)). The values of the components of the LCL filter, the distribution transformer, and the utility grid are resumed in Table 3 at left, meanwhile at right are the cutoff frequencies and damping factors of the LCL filter.

Table 3. Power Subsystem characteristics.

• R=0.0465Ω
• L=1.1mH
• C=4μF (Y-connection)
• Transformer:
  • R_t= 0.247 Ω
  • L_t= 640 μH, neglecting the magnetizing effect
• 3-phase utility grid voltage: 132.8V rms (phase-to-neutral)
	$f_c = \frac{1}{2\pi}\frac{R}{L} = 6.72Hz$	**First order RL**

	$f_o = \frac{1}{2\pi\sqrt{LC}} = 2400Hz$ $(harm = 48)$ $\zeta = \frac{\omega_o}{2}RC = 0.0014$	**Second order LC**
	$f_{ot} = \frac{1}{2\pi\sqrt{L_t C}} = 3145.6Hz$ $(harm = 63)$ $\zeta_t = \frac{\omega_o}{2}R_t C = 0.0098$	**Second order LtC**

The values of the parameters for the control subsystem and the DSOGI-FLL synchronization algorithm are resumed in Table 4:

Table 4. Control subsystem and the synchronization algorithm characteristics

- K_{INV}=400V (V_{CC}=600V)
- C_{link}=2300µF ($\Delta V_{CCmáx}$=60V)
- f_{cI}=1220.8 **(open loop cross-over frequency for the inner current loop)**
- PM_I=63.5°
- K_P =0.0211
- K_I =10
- $K_{Ih5} = K_{Ih7}$ =10
- ω_0= 314.16rad/s
- ω_c =10rad/s
- $\omega_{c5h} = \omega_{c7h}$ =10rad/s
- f_{cV}=12.2Hz **(open loop cross-over frequency for the outer dc bus voltage loop)**
- PM_V =PM_I **(phase margin for the outer and inner open loop transfer functions)**
- $\zeta_c = \sqrt{2}/2$ **(damping factor for the closed loop outer voltage loop)**
- ΔI=16.7A (S=10KVA) **(equivalent step of irradiance for the rated nominal power)**

DSOGI-FLL parameters

- k =1.41
- Γ =100

4. SIMULATIONS

In order to evaluate the control and the synchronization algorithms some simulations have been performed using the MATLAB/SIMULINK [20] model of the grid-connected PV system shown in Fig. 8. The Power Subsystem is update at $Ts_{\_Plant}$=2.56µs, meanwhile the control subsystem is updated at $Ts_{\_Controller}$= 20.478µs, and is modelled inside the Triggered Subsystem (named Vector Controller) which is driven by a signal emulating an Interrupt Request in the microcontroller. Analog PWM is used with a switching frequency F_{PWM}=12.208kHz.

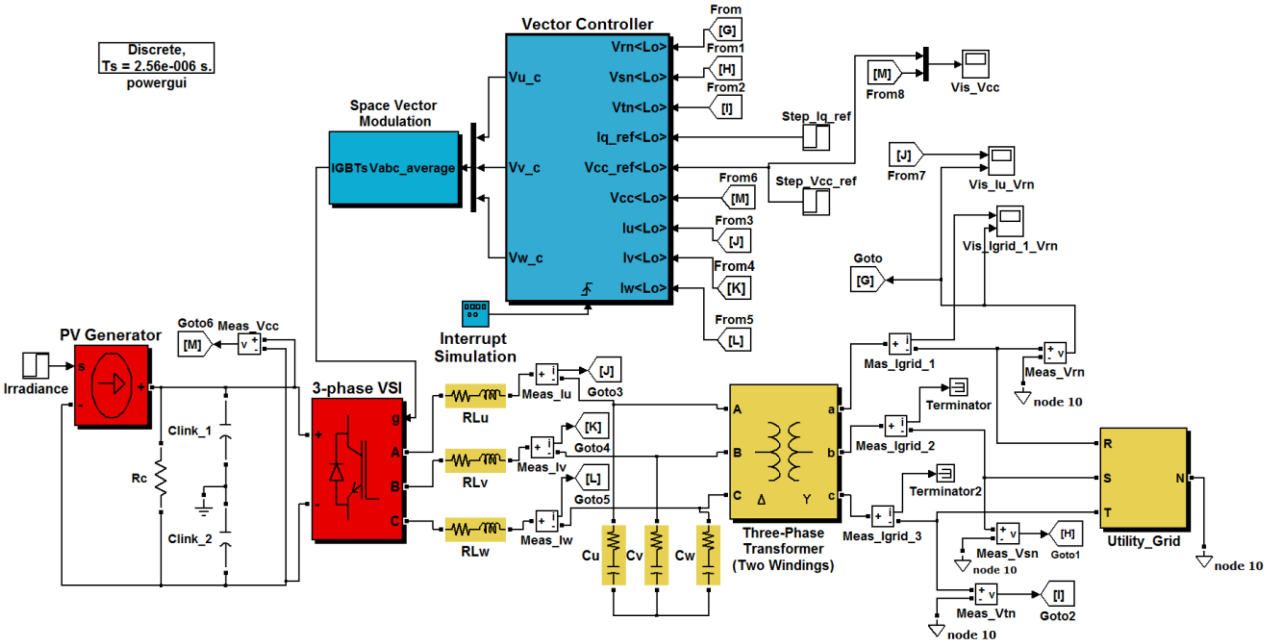

Fig. 8. SIMULINK model of the PV grid-connected system.

The SIMULINK implementation of the DSOGI-FLL synchronization algorithm together with the cascade control used in this paper are shown in Fig. 9, both included in the Vector Controller block. The cascade control is formed by the outer loop regulator that compares the dc bus voltage in the link capacitor with the reference which comes from the MPPT algorithm block[1]. This control loop has been performed using a **PI regulator**. The inner control loop uses two **PR controllers** to regulate the $\alpha\beta$ components of the line currents. A **harmonic compensator (HC) structure** is used in both PR controllers.

The detailed SIMULINK implementation of the **DSOGI-FLL** synchronization algorithm and the **FLL structure** for 3-phase systems are shown in Fig. 10a and Fig. 10b, respectively. The output phase of this module is computed by an S-**F**unction block as Eq. (10) suggests.

[1] The MPPT algorithm block is commonly a part of the PV Generator, but it is not modelled because it is out of the scope of this paper as said before. Instead, the reference to track the maximum power point is generated with the *Step_Vcc_ref* block so as to be able to test the proper behavior of the cascade control exerted.

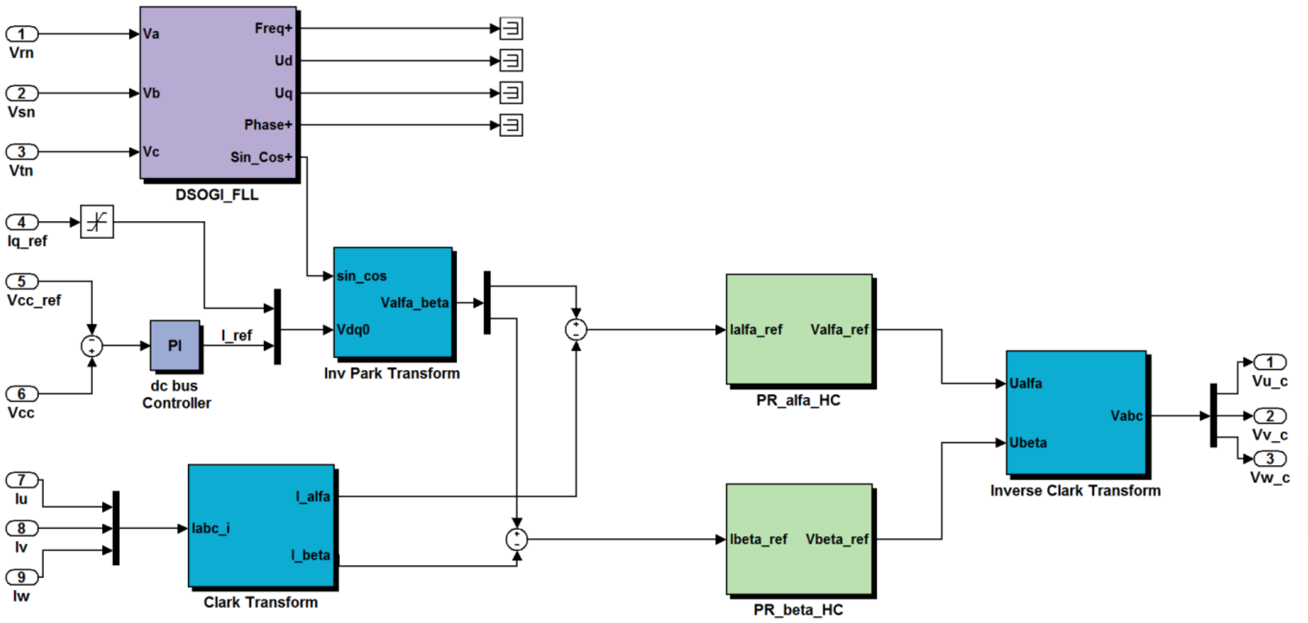

Fig. 9. SIMULINK model of the cascade control.

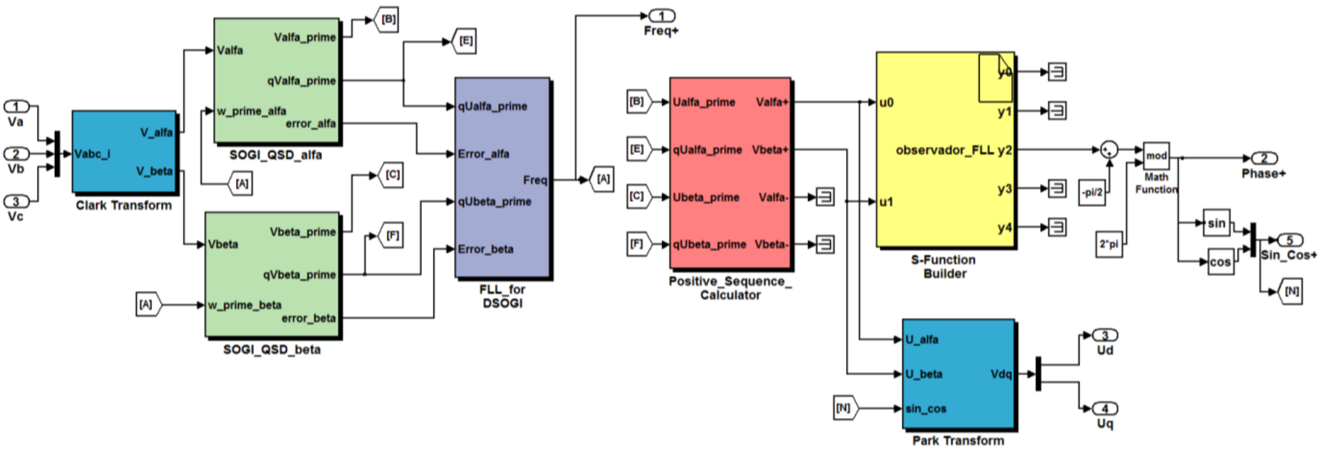

(a)

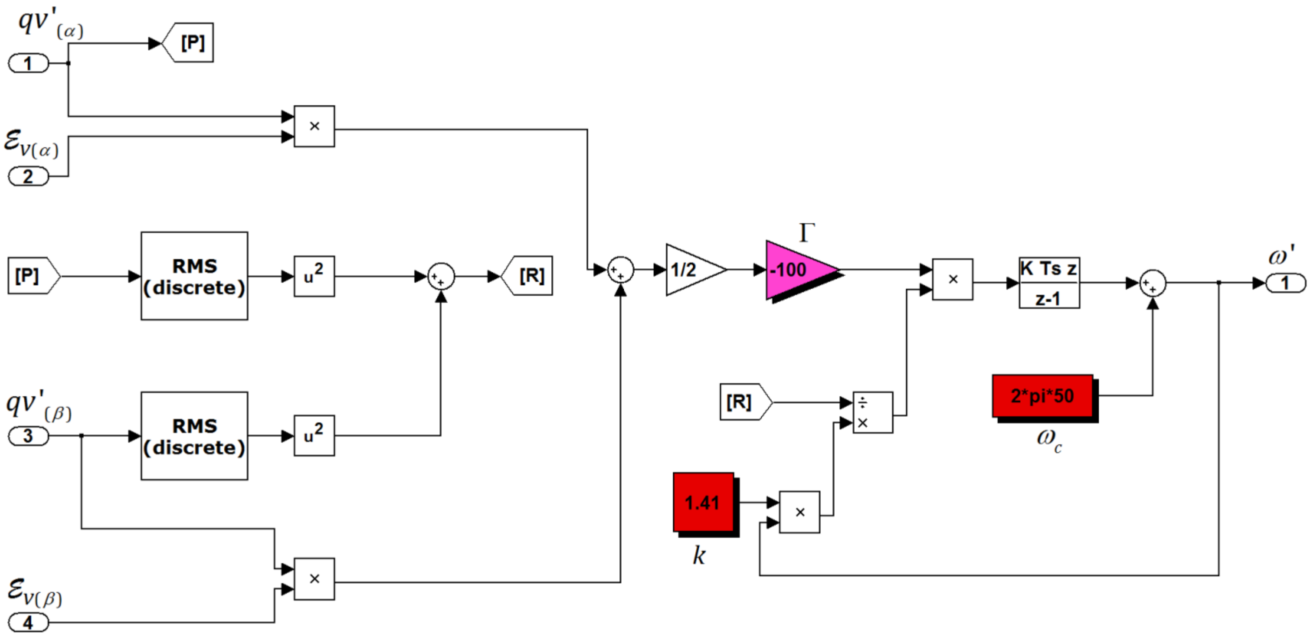

(b)

Fig. 10. a) SIMULINK model of the DSOGI-FLL synchronization algorithm.
b) SIMULINK model of the FLL structure with gain normalization.

In order to simulate the time response of the 3-phase grid-connected VSI under different input conditions several time simulations have been carried out.

The time response to a change in the MPPT of the I-V curve of the PV generator is simulated with the corresponding step from 500V to nominal value (600V) in the dc bus voltage reference V^{*}_{CC} exerted at 0.5s, and for a constant incoming output current from the PV generator for a specific irradiance; see Fig. 11a: the proper time response of the dc bus voltage regulator is shown in **red**. An overshoot less than 5% of the nominal dc bus voltage is attained, allowing the proper overvoltage protection of the link capacitor together with a fast settling time around 200ms.

Figures 11b and 11c show the time response of the voltage and grid current at phase 1, and the instantaneous active and reactive powers delivered to the 3-phase utility grid, respectively, for a variation in the incoming irradiance. For this, a step in the output current of the PV generator I_g is exerted at 0.7s from a 50% up to nominal conditions with constant dc bus voltage reference, producing the increase of the instantaneous active power from 5kW to 10kW approximately (trace in **red**), meanwhile the instantaneous reactive power is almost constant (trace in **black**).

A step of 4.4kVar is exerted in the instantaneous reactive power reference, producing the time response shown in Fig. 11d (trace in **black**), meanwhile the instantaneous active power is almost constant at 10kW (trace in **red**) due to the decoupled control exerted.

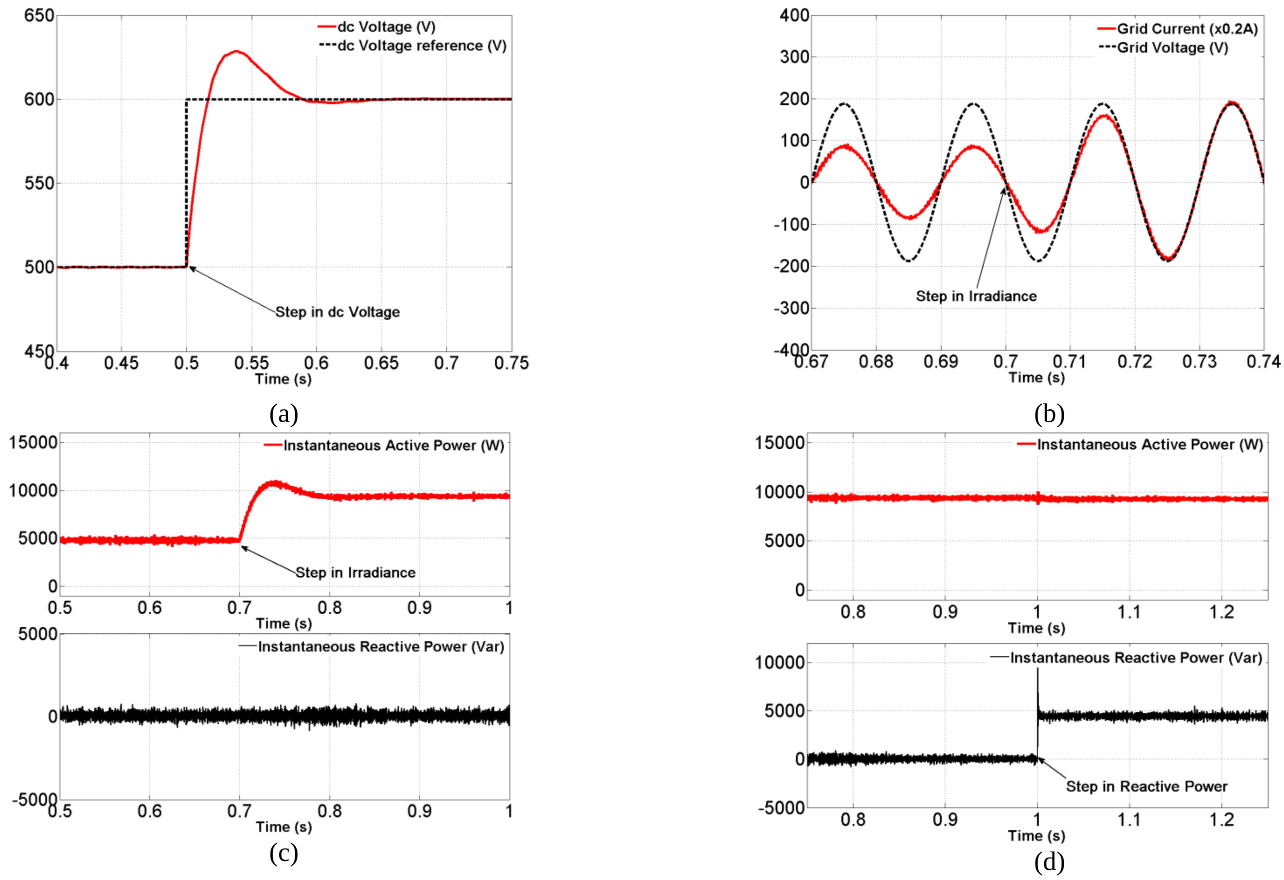

Fig. 11. a) dc bus voltage during a step in V^*_{CC} (constant output current i_p in PV modules).
b) Grid voltage and current at phase 1 during a step from 50% to nominal irradiance (constant V^*_{CC}).
c) Instantaneous active and reactive powers during a step from 50% to nominal irradiance (constant V^*_{CC}).
d) Instantaneous active and reactive powers during a step in reactive power (constant i_p and V^*_{CC}).

The new German grid code establishes that the generating power plants must be disconnected from the grid if the grid frequency is lower than 47.5 Hz or greater than 51.5 Hz, they must reduce the output instantaneous active power with a gradient of 40% of the rated power per hertz, if the grid frequency is greater than 50.2 Hz [50]. In Europe, the utility grid frequency is 50Hz and very seldom might have a variation of 49-50.3 [51].

Transient faults can produce frequency variations and for this, some simulations during a step of frequency are performed in this section so as to test the behaviour of the DSOGI-FLL synchronization algorithm: the simulation of the time evolution of the detected frequency and phase are shown in Fig. 12 in which the rms value of the 3-phase utility grid voltage is Vrms=230V (phase-to-phase) and a step of frequency from 50Hz to 60Hz is exerted at 0.5s. A reliable frequency and phase detection is attained by the DSOGI-FLL as it can be observed in Fig. 12a, and the synchronization of the voltage and current at phase 1 is perfectly attained as it is shown in Fig. 12b, producing a unitary power factor operation before and after the step.

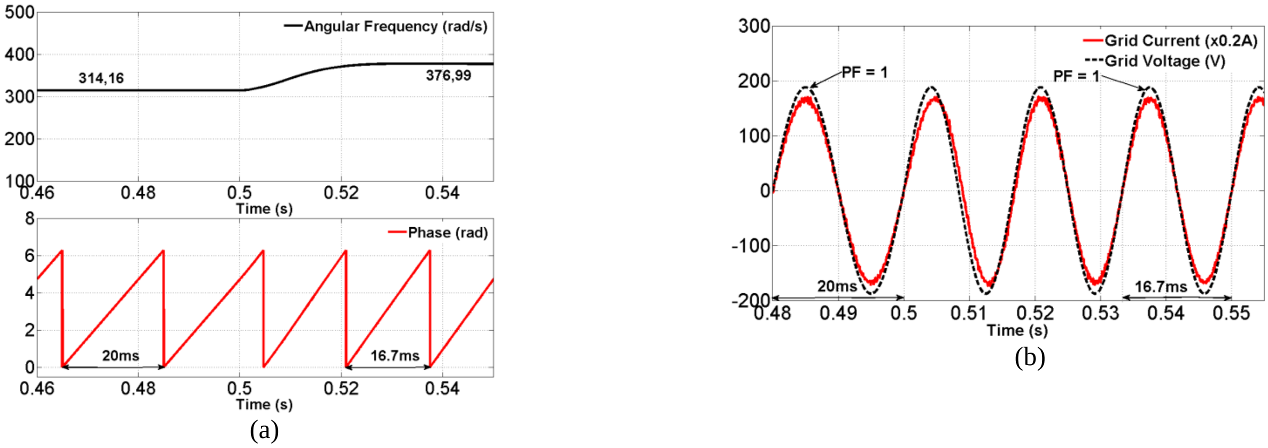

Fig. 12. a) Time evolution of the detected frequency and phase during a step of the nominal frequency.
b) Grid voltage and current at phase 1 during a step of the nominal frequency.

In order to analyze the response of the DSOGI-FLL when voltage unbalances occur in the low-voltage 3-phase utility grid, Fig. 13a shows the time evolution of the detected frequency and phase by the DSOGI-FLL algorithm for a ground fault in phase 3 (V_r=187.79V peak, V_s=187.79V peak, V_t=0 (phase-to-neutral)) where an optimal frequency and phase detection is attained (2nd order harmonic free). This optimal detection is due to the use of the PSC block that was explained in Section 2.2.1 (synchronization algorithm).

The advantages of using the PSC block in a PV grid-connected system are clearly shown in Fig. 13b: the voltage amplitudes of the 3-phase utility grid for a ground fault in phase 3 are shown in the upper zone; meanwhile the pure 3-phase sinusoidal currents are depicted in the bottom zone. This situation arises because the PSC block removes the negative sequence of the 3-phase voltages, producing a feedback phase with the equivalent positive sequence.

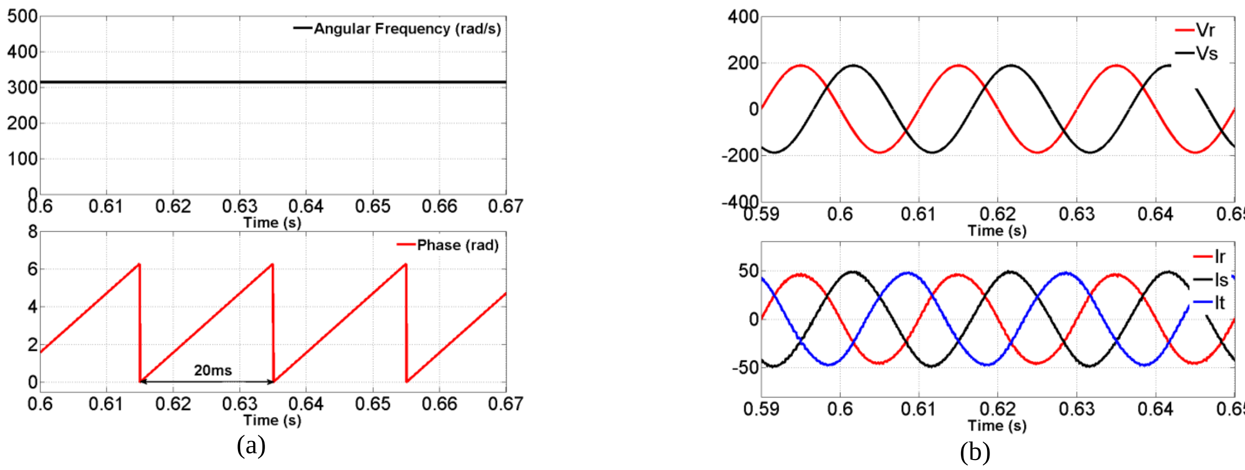

Fig. 13. a) Time evolution of the detected frequency and phase when voltage unbalances occur (ground fault in phase 3).
b) Time evolution of the grid voltages and currents when voltage unbalances occur (ground fault in phase 3).

For the next simulations, the 5th and 7th harmonics are introduced in the 3-phase utility grid voltages with an amplitude distortion of 10% for both harmonics. The frequency and phase detection by the DSOGI-FLL is shown in Fig. 14a, and because of the effects of the high harmonic pollution in the utility grid voltages, a frequency and phase detection with harmonics can be observed. The time evolution of the grid current at phase 1 is shown in Fig.14b where an important harmonic attenuation can be observed.

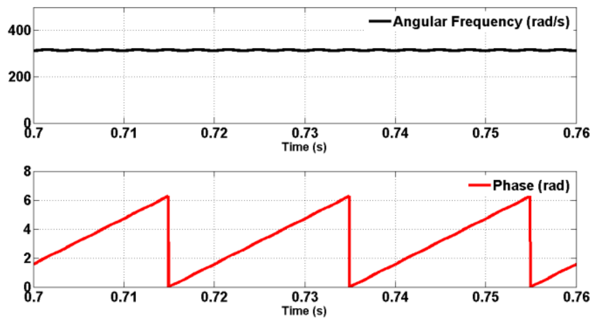

(a)

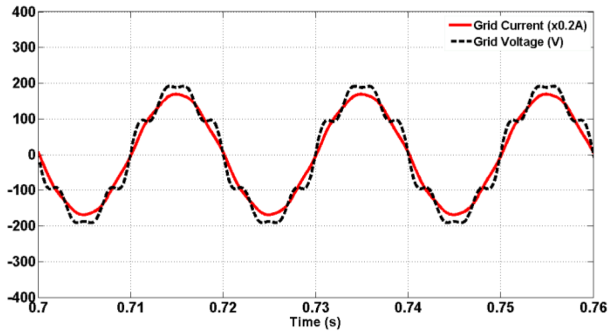

(b)

Fig. 14. a) Time evolution of the detected angular frequency and phase for a 5th and 7th harmonics distortion in the 3-phase utility grid voltages.

b) Time evolution of the grid voltage and current at phase 1**.**

5. EXPERIMENTS USING REAL-TIME DIGITAL SIMULATIONS

In order to support the results obtained with simulations, a series of real-time experiments have been carried out using a DS1006 DSPACE platform with several I/O blocks. The model blocks of the control and power subsystems are built in MATLAB/SIMULINK, the C-code is generated with Real Time Workshop and downloaded into the DSPACE platform. The platform is formed by a host PC, the DS1006 DSPACE and the DS5202 Electric Motor HIL Solution boards with digital-to-analog and analog-to-digital converters interface, as well as an oscilloscope for waveforms monitoring. The configuration of the real time platform setup is shown in Fig. 15 and a photo of the experiment setup is shown in Fig.16.

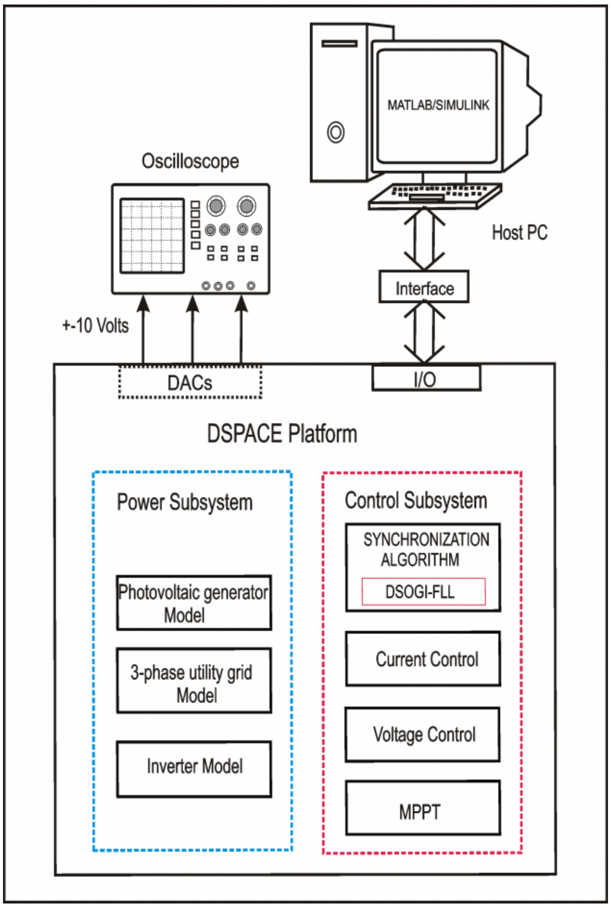

Fig. 15. Platform setup for the real-time experiments.

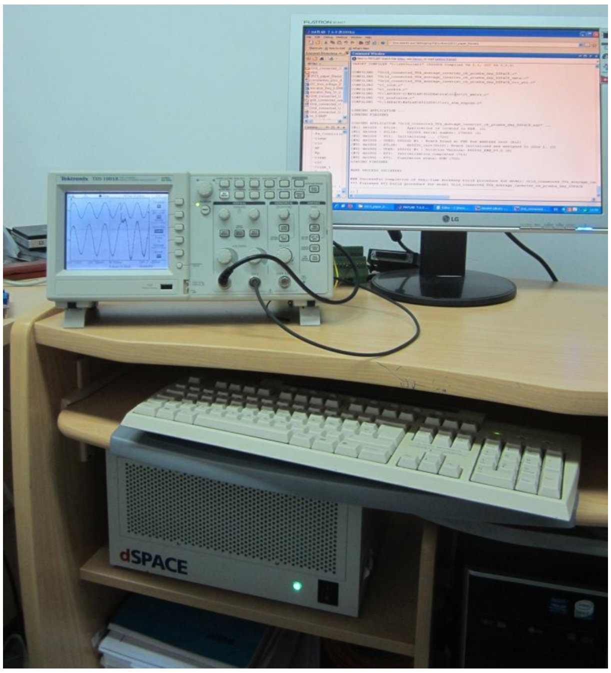

Fig. 16. Photo of the real-time digital platform setup.

5.1 Testing the control algorithm

The first real-time digital test is focused in the response of the control algorithm under different perturbations coming from the PV modules. Also a step of reactive power is exerted in order to evaluate the capability of the control strategy to deal with this type of disturbances.

The real-time response of the control to a change in the MPPT of the I-V curve of the PV generator is simulated with a corresponding step from 500V to 600V (its nominal value) in the dc bus voltage reference V^*_{CC} and keeping constant the incoming output current from the PV generator for a specific irradiance, as can be seen in Fig. 17a: the proper real-time evolution of the dc bus voltage is attained. A common situation in PV systems is a variation of the solar irradiance over the PV modules and for this, a step in the output current of the PV generator I_g is exerted from a 50% up to nominal conditions with constant dc bus voltage reference: consequently, the grid current at phase 1 also increases from 50% up to its final value as can be seen in Fig. 17b, the instantaneous active power increases from 5kW to 10kW approximately as can be observed in Fig. 17c, meanwhile the instantaneous reactive power does not vary in this condition. Figure 17d shows the real-time evolution of the instantaneous active and reactive powers injected to the 3-phase utility grid when a step of 4.4kVar is exerted; in this case, the instantaneous active power is almost constant around 10kW at steady state, due to the decoupled control exerted.

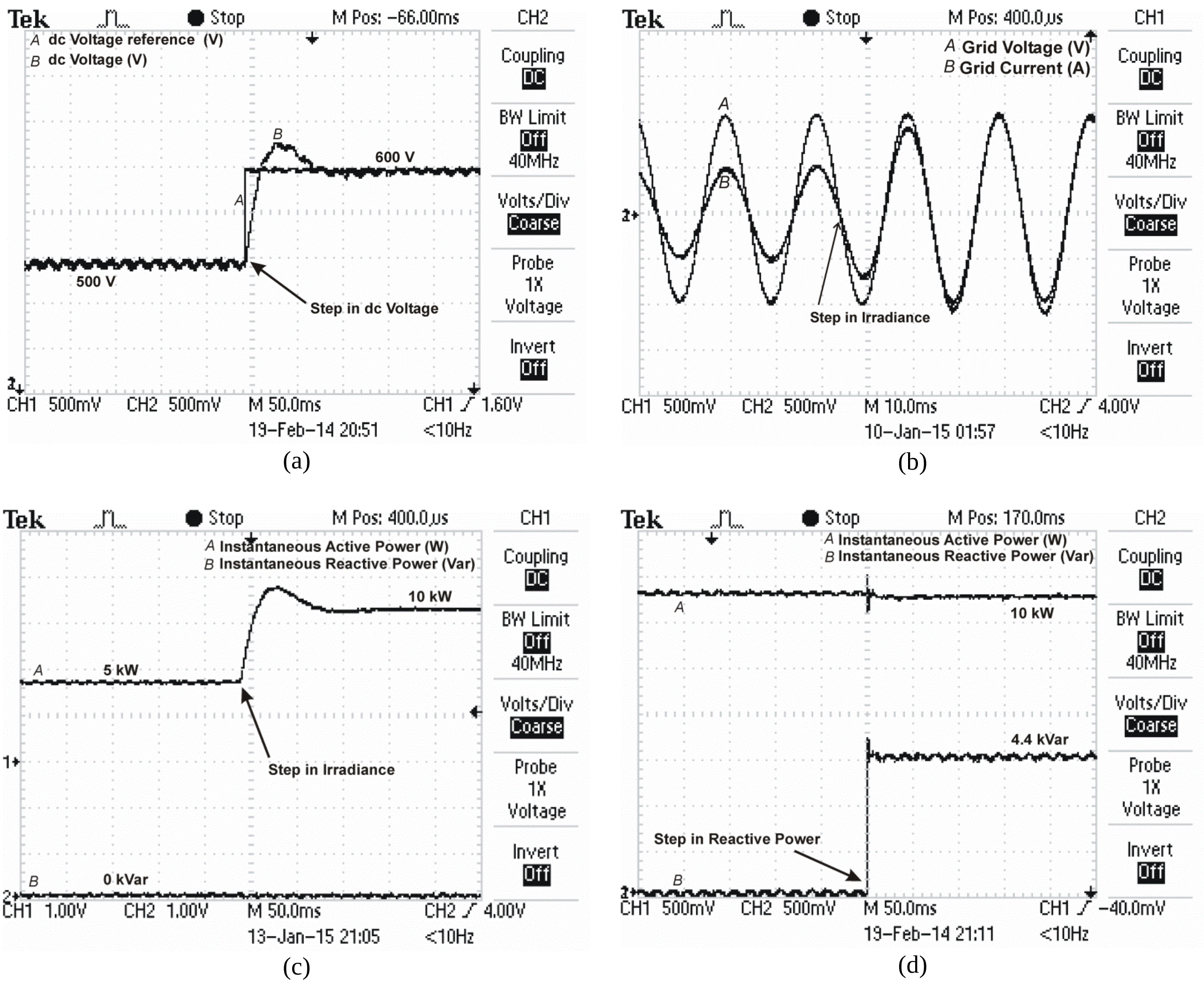

Fig. 17. a) Real-time dc bus voltage during a step in V^*_{CC} (constant output current i_p in PV modules).
b) Real-time grid voltage and current at phase 1 during a step from 50% to nominal irradiance (constant V^*_{CC}).

c) Real-time instantaneous active and reactive powers during a step from 50% to nominal irradiance (constant V^*_{CC}).
d) Real-time instantaneous active and reactive powers during a step in reactive power (constant i_p and V^*_{CC}).

5.2 Testing the influence of the nominal frequency variation

The second real-time digital test deals with the validation of the DSOGI-FLL synchronization algorithm where a step of frequency from 50Hz to 60Hz is applied. The frequency detection is shown in Fig. 18a and the time evolution of the voltage and grid current at phase 1 are depicted in Fig. 18b.

It can be seen an optimal frequency detection by this algorithm when variations of the nominal frequency of the utility grid occur, due to no power factor degradation of the inverter-grid connection happens prior and after the step of frequency, as can be seen in Fig. 18b, attaining a unitary power factor operation. These results validate the proper behaviour of the DSOGI-FLL synchronization algorithm, as an adaptive filter for the frequency variations in the utility grid voltages.

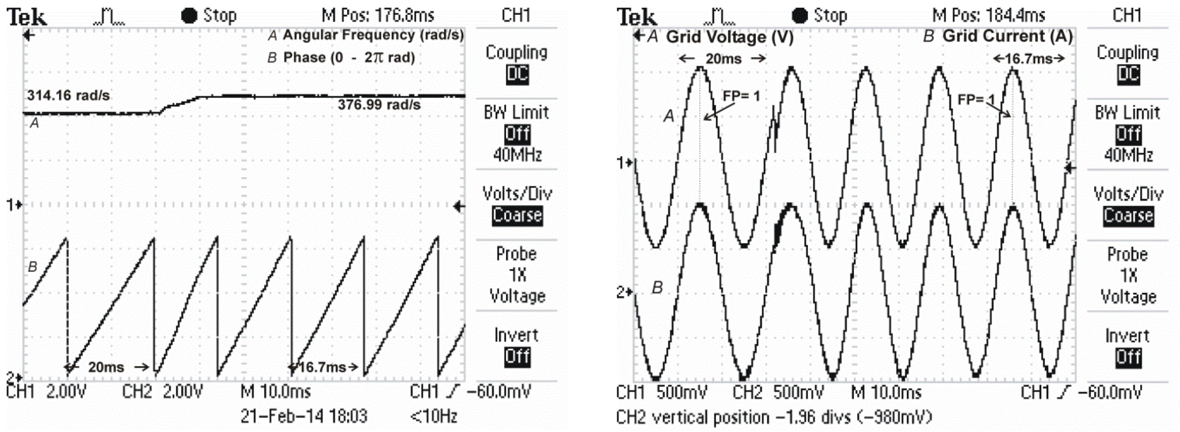

(a) (b)

Fig. 18. a) Real-time detected frequency and phase during a step of the nominal frequency.
b) Real-time grid voltage and current at phase 1 during a step of the nominal frequency.

5.3 Testing the influence of the Voltage Unbalances

The third real-time digital test has been focused in the response of the DSOGI-FLL algorithm when voltage unbalances occur in the low voltage 3-phase utility grid due to a ground fault in phase 3 (modelled as V_r=V_s=187.79V_{peak} , V_t=0V (phase-to-neutral)). Figure 19a shows the time evolution of the real-time detected frequency and phase, where a constant frequency and a pure ramp for the phase detection are attained (free of the 2nd order harmonic) as can be seen.

Figure 19b shows the real-time evolution of the grid voltage and current at phase 1. In this, the current waveform is a pure sinusoid because no negative sequence of the 3-phase voltages is feedback into the current PR controller due to the use of the PSC block in the DSOGI-FLL synchronization algorithm.

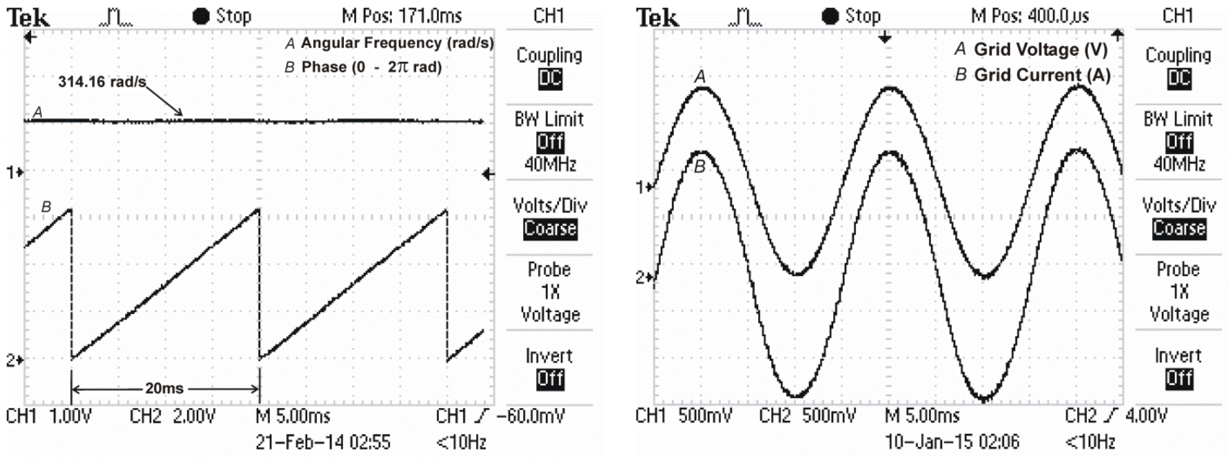

(a) (b)

Fig. 19. a) Real- time evolution of the detected frequency and phase when voltage unbalances occur (ground fault in phase 3).
b) Real-time evolution of the grid voltage and current at phase 1 when voltage unbalances occur (ground fault in phase 3).

5.4 Testing the influence of the Harmonic Distortion

The final real-time digital test has been performed with a 10% pollution in the magnitude of the low order 5^{th} and 7^{th} harmonics in the 3-phase utility grid voltages and, as a consequence, the grid currents will be affected by its influence [9]. Figure 20a displays the real-time evolution of the detected angular frequency and phase, meanwhile Fig. 20b displays the utility grid voltage and current at phase 1. The frequency spectrum of the grid current at phase 1 is depicted in Fig. 20c, where an equivalent amplitude distortion of 2.24% and 2.51% for the 5^{th} and 7^{th} harmonics (see Fig. 20d for a zoom), respectively, and a THD_I=3.36% is observed. This THD_I indicates that the system fulfill with the harmonic standards for PV system which establishes a THD_I <5% [5,8].

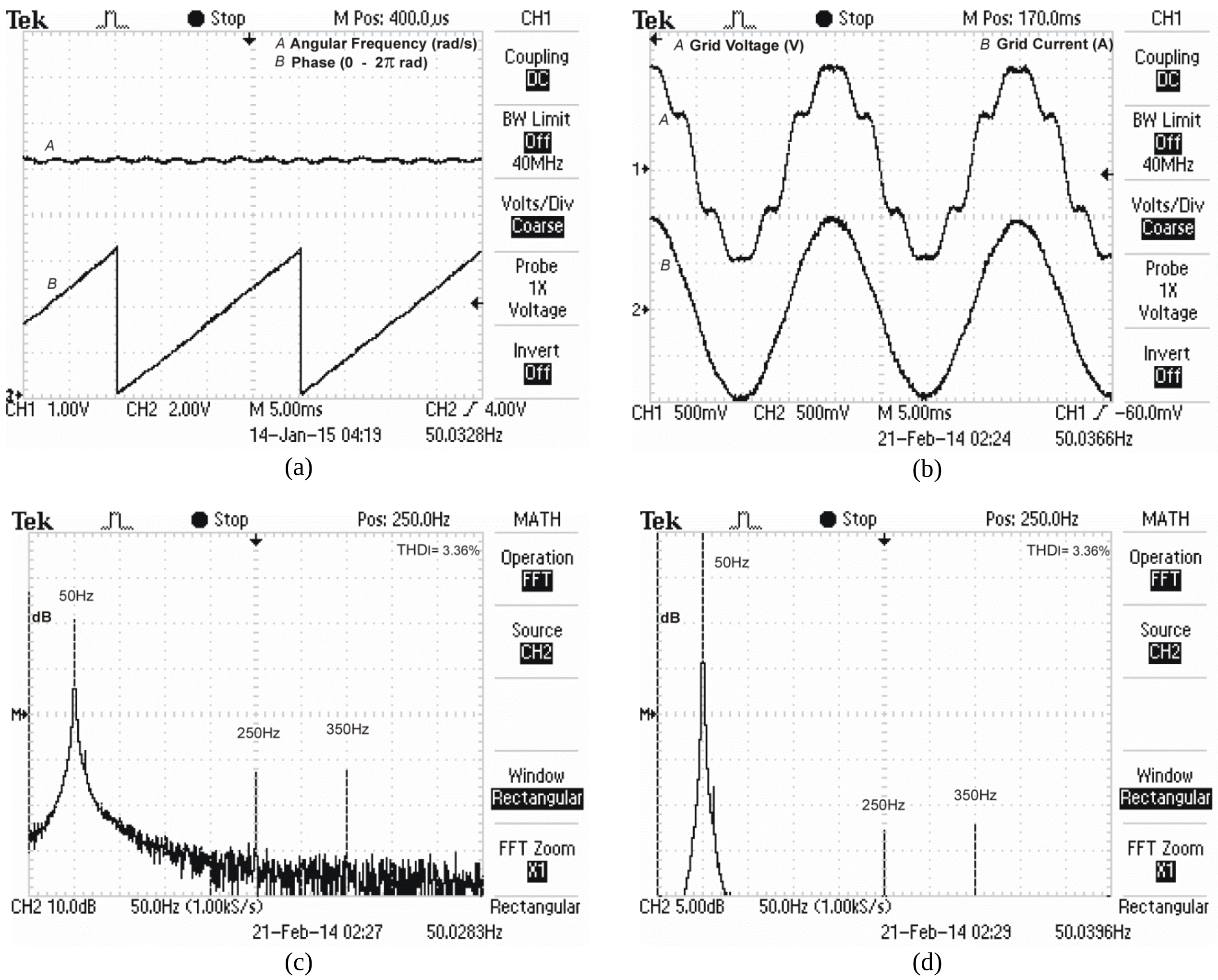

Fig. 20. a) Real-time evolution of the detected angular frequency and phase for a 5th and 7th harmonics distortion in the 3-phase utility grid voltages.
b) Real-time evolution of the grid voltage and current at phase 1.
c) Frequency spectrum of the grid current at phase 1.
d) Zoom of the frequency spectrum for the grid current at phase 1.

A resume of the harmonic distortions of the current at phase 1 and its comparison with the limits imposed by the normative [5,8] are shown in Table 5.

Table 5. Harmonic Distortions for the grid current at phase 1

Odd harmonics	Harmonic Distortion	Distortion limit
5th	2.24%	< **4.0%**
7th	2.51%	< **4.0%**
	THD_I	THD_I limit
	3.36%	< **5.0%**

6. CONCLUSIONS

In this paper the parameters for the **combined operation** of the control and the synchronization algorithms have been chosen in order to obtain the appropriate performance of the grid-connected PV system when some perturbations as harmonic pollution, voltage unbalances and frequency variations are present. The power factor control and the power quality have been the main characteristics for the evaluation of this performance.

The DSOGI-FLL synchronization algorithm has been studied in detail, and its performance for several gains is analyzed, yielding an optimal value for guaranteeing a trade-off between the settling time, overshoot and harmonic rejection:

1) An unitary power factor operation is attained when frequency variations occur due to its capability of estimating the adequate phase and frequency as an adaptive filter performance.
2) When voltage unbalances occur, this algorithm is able to calculate the positive sequence of the utility grid voltages ensuring a distorted-free feedback phase and hence, the current controller will be able to feed the 3-phase currents into the utility grid with no second order harmonic distortion.
3) The adaptive filter structure is tuned to the nominal frequency of the utility grid and can produce a high rejection to the amplitude of the harmonic components in the utility grid, reducing also the resulting distortion of the feedback phase angle.

A Proportional Resonant (PR) controller has been used in the inner current loop in order to obtain zero error in steady state for sinusoidal input signals, and a Harmonic Compensator (HC) structure has been incorporated into this control strategy in order to obtain the 3-phase voltage references for the PWM block with no harmonic contamination. In this paper, the validation of this issue has been carried out by introducing an amplitude distortion in the 5^{th} and 7^{th} harmonics of the utility grid voltages, which finally lead to the injection of good power quality into the utility grid according to international standards.

Acknowledgements

This work has been supported by a grant from La Fundación Séneca, Agencia de Ciencia y Tecnología de la Región de Murcia, Spain, as a part of the Project Ref.11948/PI/09, entitled “Design and construction of a hardware/software prototype for the synchronization and monitoring of renewable agents in a Distributed Generation System” (Alexis. B. Rey-Boué), and a scholarship towards the PhD degree from the Universidad Politécnica de Cartagena, Spain, with the Santander Bank support (N. F. Guerrero-Rodríguez).

Appendix A

For a 3-phase system described by vector $\mathbf{x}=[x_a\ x_b\ x_c]^t$, where x_a, x_b, and x_c are instantaneous 3-phase variables and ^{t} means transpose, the Clarke and Park transformations [13] are defined in (A.1) and (A.2), respectively:

$$\begin{bmatrix} x_o \\ x_\alpha \\ x_\beta \end{bmatrix} = \sqrt{\frac{2}{3}} \begin{bmatrix} \frac{1}{\sqrt{2}} & \frac{1}{\sqrt{2}} & \frac{1}{\sqrt{2}} \\ 1 & -\frac{1}{2} & -\frac{1}{2} \\ 0 & \frac{\sqrt{3}}{2} & -\frac{\sqrt{3}}{2} \end{bmatrix} \begin{bmatrix} x_a \\ x_b \\ x_c \end{bmatrix} \tag{A.1}$$

where x_0 is the zero-sequence component and $x_{\alpha,\beta}$ are the αβ components of vector **x** in the stationary reference frame.

$$\begin{bmatrix} x_d \\ x_q \end{bmatrix} = \begin{bmatrix} \cos\theta & \sin\theta \\ -\sin\theta & \cos\theta \end{bmatrix} \begin{bmatrix} x_\alpha \\ x_\beta \end{bmatrix} \tag{A.2}$$

where $x_{d,q}$ are the dq components of vector **x** in the synchronous reference frame, and θ is the phase angle of the 3-phase utility grid voltages.

The inverse problem is also possible by computing the inverse to the above matrices, yielding the inverse Clarke and Park transformations in (A.3) and (A.4), respectively.

$$\begin{bmatrix} x_a \\ x_b \\ x_c \end{bmatrix} = \sqrt{\frac{2}{3}} \begin{bmatrix} \frac{1}{\sqrt{2}} & 1 & 0 \\ \frac{1}{\sqrt{2}} & -\frac{1}{2} & \frac{\sqrt{3}}{2} \\ \frac{1}{\sqrt{2}} & -\frac{1}{2} & -\frac{\sqrt{3}}{2} \end{bmatrix} \begin{bmatrix} x_o \\ x_\alpha \\ x_\beta \end{bmatrix} \tag{A.3}$$

$$\begin{bmatrix} x_\alpha \\ x_\beta \end{bmatrix} = \begin{bmatrix} \cos\theta & -\sin\theta \\ \sin\theta & \cos\theta \end{bmatrix} \begin{bmatrix} x_d \\ x_q \end{bmatrix} \tag{A.4}$$

References

[1] S.Ruiz-Romero, A.Colmenar-Santos, R.Gild-Ortego, and A.Molina-Bonilla, Distributed generation: The definitive boost for renewable energy in spain, Renewable Energy, 53 (2013) 354-364.

[2] M.A.Abdullah, A.P.Agalgaonkar, and K.M.Muttaqi, Climate change mitigation with integration of renewable energy resources in the electricity grid of New South Wales, Australia, Renewable Energy, 66 (2014) 305-313.

[3] IEEE Recommended Practice for Utility Interface of Photovoltaic (PV) Systems. IEEE Std 929-2000 . 2000.

[4] A.Menti, T.Zacharias, and J.Milias-Argitis, Harmonic distortion assessment for a single-phase grid-connected photovoltaic system, Renewable Energy, 36 (2011) 360-368.

[5] IEC 61727 Ed. 2, Photovoltaic (PV) Systems-Characteristics of the Utility Interface, 2004.

[6] European Committee for Electrotechnical Standardization (CENELEC), EN 50160, Voltage characteristics of electricity supplied by public distribution systems. 1999.

[7] Standard for Interconnecting Distributed Resources with Electric Power Systems, 2003.

[8] Recommended Practices and Requirements of Harmonic Control in Electrical Power Systems. Standard ANSI/IEEE 519-1992. 1992.

[9] R.Ekstrom and M.Leijon, Lower order grid current harmonics for a voltage-source inverter connected to a distorted grid, Electric Power Systems Research, 106 (2014) 226-231.

[10] Bae Youngsang, Vu Trung-Kien, and Kim Rae-Young, Implemental Control Strategy for Grid Stabilization of Grid-Connected PV System Based on German Grid Code in Symmetrical Low-to-Medium Voltage Network, IEEE Transactions on Energy Conversion, 28 (2013) 619-631.

[11] Y.Abdel-Rady, I.Mohamed, and F.El-Saadany, A Robust Natural-Frame-Based Interfacing Scheme for Grid-Connected Distributed Generation Inverters, IEEE Transactions on Energy Conversion, 26 (2011) 728-736.

[12] F.Blaabjerg, Z.Chen, and S.B.Kjaer, Power electronics as efficient interface in dispersed power generation systems, IEEE Transactions on Power Electronics, 19 (2004) 1184-1194.

[13] R.Teodorescu, M.Liserre, and P.Rodriguez, Grid Converters for Photovoltaic and Wind Power Systems. 2011. United Kingdom, John Wiley & Sons, Ltd.

[14] G.Tsengenes and G.Adamidis, Investigation of the behavior of a three phase grid-connected photovoltaic system to control active and reactive power, Electric Power Systems Research, 81 (2011) 177-184.

[15] D.Boroyevich, I.Cvetkovic, R.Burgos, and D.Dong, Intergrid: A Future Electronic Energy Network?, IEEE Journal of Emerging and Selected Topics in Power Electronics, 1 (2013).

[16] R.Teodorescu, F.Blaabjerg, M.Liserre, and PC.Loh, Proportional-resonant controllers and filters for grid-connected voltage-source converters, IEE Procedings Electric Power Applications, 153 (2006) 750-762.

[17] R.Teodorescu and F.Blaabjerg, Proportional-Resonant Controllers. A New Breed of Controllers Suitable for Grid-Connected Voltage-Source Converters. International Conference on Optimization of Electrical and Electronic Equipments. Optim 2004 , 9-14. 2004.

[18] P.Rodriguez, A.Luna, M.Ciobotaru, R.Teodorescu, and F.Blaabjerg, Advanced Grid Synchronization System for Power Converters under Unbalanced and Distorted Operating Conditions. IEEE Industrial Electronics, IECON. 5173-5178. 6-11-2006.

[19] A.V.Timbus, M.Liserre, R.Teodorescu, P.Rodriguez, and F.Blaabjerg, Evaluation of Current Controllers for Distributed Power Generation Systems, IEEE Transactions on Power Electronics, 24 (2009) 654-664.

[20] MATLAB/SIMULINK. The MathWorks, Inc. <http://www.mathworks.com/>. 2008.

[21] A.B.Rey-Boué, R.García-Valverde, F.Ruz-Vila, and J.M.Torrelo-Ponce, An integrative approach to the design methodology for 3-phase power conditioners in Photovoltaic Grid-Connected systems, Energy Conversion and Management, 56 (2012) 80-95.

[22] H.Akagi, E.Hirokazu Watanabe, and M.Aredes, Instantaneous Power Theory and Applications to Power Conditioning, John Wiley & Sons, 2007.

[23] V.Scarpa, S.Buso, and G.Spiazzi, Low-Complexity MPPT Technique Exploiting the PV Module MPP Locus Characterization, IEEE Transactions on Industrial Electronics, 56 (2009) 1531-1538.

[24] N.Mutoh, M.Ohno, and T.Inoue, A method for MPPT control while searching for parameters corresponding to weather conditions for PV generation systems. IECON 2004. 30th Annual Conference of IEEE. 3, 3094-3099. 2-11-2004.

[25] E.Clarke, Circuit Analysis of AC Power Systems, vol. I, Wiley, 1950.

[26] H.Akagi, Y.Kanazawa, and A.Nabae, Instantaneous Reactive Power Compensators Comprising Switching Devices without Energy Storage Components. IEEE Transactions on Industry Applications IA-20[3], 625-630. 1984.

[27] MP.Kazmierkowski, R.Krishnan, and F.Blaabjerg, Control in Power Electronics, Selected Problems, 2002.

[28] J.C.Hernández, J.Ortega, .De la Cruz, and D.Vera, Guidelines for the technical assessment of harmonic, flicker and unbalance emission limits for PV-distributed generation, Electric Power Systems Research, 81 (2011) 1247-1257.

[29] E.J.Bueno, F.Espinosa, F.J.Rodriguez, J.Urefi, and S.Cobrece, Current control of voltage source converters connected to the grid through an LCL-filter, Power Electronics Specialists Conference, 2004 IEEE 35th Annual, 1 (2004) 68-73.

[30] D.Hamza, Q.Mei, and P.K.Jain, Implementation of an EMI active filter in grid-tied PV micro-inverter controller and stability verification. IECON. 477-482. 25-10-2012.

[31] S.Wang, C.Xu, and H.Qin, Design theory and implementation of planar EMI filter based on annular integrated inductor-capacitor unit. Electromagnetic Compatibility (APEMC). 129-132.

[32] C.Po-Shen and L.Yen-Shin, Effective EMI Filter Design Method for Three-Phase Inverter Based Upon Software Noise Separation, IEEE Transactions on Power Electronics, 25 (2010) 2797-2806.

[33] R.Kadri, J.P.Gaubert, and G.Champenois, An Improved Maximum Power Point Tracking for Photovoltaic Grid-Connected Inverter Based on Voltage-Oriented Control, IEEE Transactions on Industrial Electronics, 58 (2011) 66-75.

[34] N.S.D'Souza, L.A.C.Lopes, and X.Liu, Comparative study of variable size perturbation and observation maximum power point trackers for PV systems, Electric Power Systems Research, 80 (2010) 296-305.

[35] K.Ishaque and Z.Salam, A review of maximum power point tracking techniques of PV system for uniform insolation and partial shading condition, Renewable and Sustainable Energy Reviews, 19 (2013) 475-488.

[36] C.B.Salah and M.Ouali, Comparison of fuzzy logic and neural network in maximum power point tracker for PV systems, Electric Power Systems Research, 81 (2011) 43-50.

[37] J.Qi, Y.Zhang, and Y.Chen, Modeling and maximum power point tracking (MPPT) method for PV array under partial shade conditions, Renewable Energy, 66 (2014) 337-345.

[38] H.Heydari-doostabad, R.Keypour, M.Reza Khalghani, and M.Hassan Khooban, A new approach in MPPT for photovoltaic array based on Extremum Seeking Control under uniform and non-uniform irradiances, Renewable Energy, 94 (2013) 28-36.

[39] A.I.Dounis, P.Kofinas, C.Alafodimos, and D.Tseles, Adaptive fuzzy gain scheduling PID controller for maximum power point tracking of photovoltaic system, Renewable Energy, 60 (2013) 202-214.

[40] V.Kaura and V.Blasko, Operation of a phase locked loop system under distorted utility conditions, IEEE Transactions on Industry Applications, 33 (1997) 58-63.

[41] F.Blaabjerg, R.Teodorescu, M.Liserre, and A.V.Timbus, Overview of Control and Grid Synchronization for Distributed Power Generation Systems, IEEE Transactions on Industrial Electronics, 53 (2006) 1398-1409.

[42] C.L.Fortescue, Method of Symmetrical Co-Ordinates Applied to the Solution of Polyphase Networks, American Institute of Electrical Engineers, XXXVII (1918) 1027-1140.

[43] M.Karimi-Ghartemani and M.R.Iravani, A method for synchronization of power electronic converters in polluted and variable-frequency environments, IEEE Transactions on Power Systems, 19 (2004) 1263-1270.

[44] P.Rodriguez, R.Teodorescu, I.Candela, A.V.Timbus, M.Liserre, and F.Blaabjerg, New Positive-sequence Voltage Detector for Grid Synchronization of Power Converters under Faulty Grid

Conditions. Power Electronics Specialists Conference, 2006. PESC '06. 37th IEEE. 1-7. 18-6-2006.

[45] Y.Xiaoming, W.Merk, H.Stemmler, and J.Allmeling, Stationary-frame generalized integrators for current control of active power filters with zero steady-state error for current harmonics of concern under unbalanced and distorted operating conditions, IEEE Transactions on Industry Applications, 38 (2002) 523-532.

[46] G.F.Franklin, J.D.Powell, and A.Emami-Naeini, Feedback Control of Dynamic Systems, Prentice-Hall,Inc., New Jersey, 2002.

[47] W.V Lyon, Applications of the method of symmetrical components, McGraw-Hill, New York, 1937.

[48] S.Buso and P.Mattavelli, Digital Control in Power Electronics, Morgan & Claypool, 2006.

[49] F.Almonacid, C.Rus, L.Hontoria, and F.J.Muñoz, Characterisation of PV CIS module by artificial neural networks. A comparative study with other methods, Renewable Energy, 35 (2010) 973-980.

[50] E.Tröster, New German Grid Codes for Connecting PV Systems to the Medium Voltage Power Grid. 2nd International Workshop on Concentrating Photovoltaic Power Plants: Optical Design, Production, Grid Connection, Darmstadt, Germany. 2009.

[51] T.Ackermann, Wind Power in Power Systems , John Wiley & Sons, Ltd., England, 2005.